Tau neutrino deep inelastic charged current interactions

S. Kretzer
Department of Physics and Astronomy, Michigan State University, East Lansing, Michigan 48824

M. H. Reno
Department of Physics and Astronomy, University of Iowa, Iowa City, Iowa 52242

(Received 22 August 2002; published 27 December 2002)

The $\nu_\mu \to \nu_\tau$ oscillation hypothesis will be tested through ν_τ production of τ in underground neutrino telescopes as well as long-baseline experiments. We provide the full QCD framework for the evaluation of tau neutrino deep inelastic charged current (CC) cross sections at leading twist, including next-to-leading-order (NLO) corrections, charm production, tau threshold, and target mass effects in the collinear approximation. We investigate the violation of the Albright-Jarlskog relations for the structure functions $F_{4,5}$ which occur only in heavy lepton (τ) scattering. Integrated CC cross sections for neutrino-nucleon interactions are evaluated naively over the full phase space and with the inclusion of DIS kinematic cuts. Uncertainties in our evaluation based on scale dependence, PDF errors and the interplay between kinematic and dynamical power corrections are discussed and/or quantified.

DOI: 10.1103/PhysRevD.66.113007 PACS number(s): 13.15.+g, 12.15.Ji, 12.38.Bx

I. INTRODUCTION

Results from the Super-Kamiokande underground experiment measuring the atmospheric neutrino flux suggest that muon neutrinos oscillate into tau neutrinos with nearly maximal mixing [1]. A test of the oscillation hypothesis is ν_τ production of τ through charged current interactions, a process which will be studied in underground neutrino telescopes [2] as well as long-baseline experiments [3] measuring neutrino fluxes from accelerator sources. For precision measurements of oscillation mixing angles and eventually *CP* violation, neutrino cross sections will ideally be known to the level of a few percent. Eventually, measurements of neutrino-nucleon charged current interaction cross sections are expected to be at the 1% level at a neutrino factory [4].

The QCD theory of deep inelastic cross sections in the leading-twist approximation has proceeded to the point of evaluating next-to-next-to-leading order (2 loop) perturbative QCD corrections to the coefficient functions for the structure functions F_1, F_2 and F_3 [5–8] and approximations for the splitting functions [9–11]. In the specific case of ν_μ-isoscalar nucleon (N) cross sections, target mass corrections and nuclear binding effects in a leading order (LO) twist-2 approach of deep inelastic scattering (DIS), combined with the elastic peak and a modeling of higher twists in the continuum and resonance region of DIS, have also been investigated [12,13]. Tau neutrino charged current interactions with nucleons have received less theoretical attention [12,14,15]. Albright and Jarlskog, in Ref. [16], pointed out that there are two additional structure functions, F_4 and F_5, that contribute to the tau neutrino cross section. F_4 and F_5 are ignored in muon neutrino interactions because of a suppression factor depending on the square of the charged lepton mass (m_ℓ) divided by the nucleon mass times neutrino energy, $m_\ell^2/(M_N E_\nu)$. At leading order, in the limit of massless quarks and target hadrons, F_4 and F_5 are

$$F_4 = 0 \tag{1}$$

$$2xF_5 = F_2, \tag{2}$$

where x is the Bjorken-x variable. These generalizations of the Callan-Gross relation $F_2 = 2xF_1$ are called the Albright-Jarlskog relations. As with the Callan-Gross relations, the Albright-Jarlskog relations are violated from kinematic mass corrections and at next LO (NLO)[1] in QCD. We quantify the violation in Sec. III A.

Below $E_\nu \sim 10$ GeV for muon neutrinos and higher energies for tau neutrinos, untangling the exclusive and inclusive contributions to the neutrino-nucleon cross section is difficult. The cross section in this energy range has quasi-elastic, resonant production (such as Δ production), nonresonant pion production and other inelastic contributions. There are several phenomenological methods for avoiding double counting in this region. One method employs a cutoff in the hadronic invariant mass $W > W_{\rm min}$ such that the combined exclusive and $W_{\rm min}$ dependent inclusive cross section yields a total consistent with data [17]. Using muon neutrino data, a common choice for $W_{\rm min}$ is 1.4 GeV. A second method involves looking at different final state multiplicities [14]. By normalizing the calculated total cross section for a given multiplicity j, $\sigma^j_{\rm tot}$, to the data, one can determine the factors f_j in $\sigma^j_{\rm tot} = \sigma^j_{\rm res} + f_j \sigma^j_{\rm DIS}$. The quantity $\sigma^j_{\rm DIS}$ is determined by the inelastic cross section and the hadronization scheme. The Monte Carlo program for the Soudan experiment does the normalization at $E_\nu = 20$ GeV [14].

We present here the deep-inelastic contribution to $\nu_\tau N \to \tau X$ incorporating next-to-leading order QCD corrections, collinear target mass and charmed quark mass corrections. As explained above, our results for the leading twist DIS component only approximate the full cross section in the low energy region of $E_\nu < 20$ GeV where quasi-elastic and reso-

[1] We will find below that Eq. (2) is *not* violated in *massless* NLO QCD.

nant scattering play important roles in ν_τ scattering [18–20] and must be investigated in greater detail. Charm mass corrections are included for consistency in keeping tau mass and target mass corrections. The NLO structure functions F_4 and F_5 including charm quark production have been evaluated by Gottschalk in Ref. [21]. Here, we correct a misprint and evaluate gluonic helicity states in D dimensions rather than 4 dimensions. We show numerical results for the new structure functions and for the charged current cross sections, both with and without imposing a nonzero value for $W_{\rm min}$. To gauge the effects of perturbative delicacies such as higher-twist beyond the inclusion of target mass effects in the scaling variable, we also evaluate the effect of imposing a cutoff on Q^2. We find that the collinear cutoff effect of the tau mass $m_\tau = 1.78$ GeV is enough to guarantee that for $E_{\nu_\tau} \gtrsim 5$ GeV, $\sigma_{\rm CC}(\nu_\tau N)$ is dominated by $Q^2 > 1$ GeV^2. While this is widely considered a perturbative scale in QCD, some caveats about the possible importance of higher twist are discussed.

In Sec. II, we show the formulas for the differential cross section in terms of structure functions, and the expressions for the structure functions at NLO. Charm quark mass corrections for the charged current process are displayed, together with the results for the $m_c \to 0$ limit. In Sec. III, we exhibit our numerical results for the structure functions F_4 and F_5, and for $\nu_\tau N$ and $\overline{\nu}_\tau N$ interactions for neutrino energies up to 100 GeV. Cross sections are compared to those with incident muon neutrinos and uncertainties are discussed. We conclude in Sec. IV. In an Appendix we rewrite the Albright-Jarlskog relations in terms of helicity amplitudes and pinpoint the approximations in their derivation.

II. ν_τ DIS AT NLO

Neglecting neither the target nucleon mass M_N nor the final state lepton mass m_τ, the charged current ν_τ (anti-)neutrino differential cross section is represented by a standard set of 5 structure functions [16],[2]

$$\begin{aligned}\frac{d^2\sigma^{\nu(\overline{\nu})}}{dxdy} = \frac{G_F^2 M_N E_\nu}{\pi(1+Q^2/M_W^2)^2} \Bigg\{ & \left(y^2 x + \frac{m_\tau^2 y}{2E_\nu M_N}\right) F_1^{W^\pm} \\ & + \left[\left(1 - \frac{m_\tau^2}{4E_\nu^2}\right) - \left(1 + \frac{M_N x}{2E_\nu}\right) y\right] F_2^{W^\pm} \\ & \pm \left[xy\left(1 - \frac{y}{2}\right) - \frac{m_\tau^2 y}{4E_\nu M_N}\right] F_3^{W^\pm} \\ & + \frac{m_\tau^2 (m_\tau^2 + Q^2)}{4E_\nu^2 M_N^2 x} F_4^{W^\pm} - \frac{m_\tau^2}{E_\nu M_N} F_5^{W^\pm} \Bigg\}, \end{aligned} \tag{3}$$

where $\{x, y, Q^2\}$ are the standard DIS kinematic variables related through $Q^2 = 2M_N E_\nu xy$ and where we have neglected factors of $m_\tau^2/2M_N E_\nu \cdot Q^2/M_W^2$. These latter corrections from the $\sim q^\mu q^\nu / M_W^2$ part of the massive boson propagator are negligible both at low and at high neutrino energies and will not enter our numerics. For completeness of this formulary, though, they can be included multiplicatively by replacing

$$F_i^{W^\pm} \to F_i^{W^\pm} \times (1 + \epsilon_i) \tag{4}$$

with

$$\begin{aligned} \epsilon_1 &= \frac{m_\tau^2 (Q^2 + 2M_W^2)}{2M_W^4} \\ \epsilon_2 &= -\frac{E_\nu^2 m_\tau^2 y [4M_W^2 + y(Q^2 + m_\tau^2)]}{M_W^4 [4(y-1)E_\nu^2 + m_\tau^2 + Q^2]} \\ \epsilon_3 &= 0 \\ \epsilon_4 &= \frac{Q^2 (Q^2 + 2M_W^2)}{M_W^4} \\ \epsilon_5 &= \frac{Q^2}{M_W^2} + \frac{(M_W^2 + Q^2)(m_\tau^2 + Q^2) y}{2M_W^4}. \end{aligned} \tag{5}$$

Kinematics determine the integration ranges[3] to be [12,16]

$$\frac{m_\tau^2}{2M_N(E_\nu - m_\tau)} \leqslant x \leqslant 1 \tag{6}$$

and

$$a - b \leqslant y \leqslant a + b \tag{7}$$

where

$$\begin{aligned} a &= \frac{1 - m_\tau^2 \left(\dfrac{1}{2M_N E_\nu x} + \dfrac{1}{2E_\nu^2}\right)}{2\left(1 + \dfrac{M_N x}{2E_\nu}\right)} \\ b &= \frac{\sqrt{\left(1 - \dfrac{m_\tau^2}{2M_N E_\nu x}\right)^2 - \dfrac{m_\tau^2}{E_\nu^2}}}{2\left(1 + \dfrac{M_N x}{2E_\nu}\right)}. \end{aligned} \tag{8}$$

In the perturbative regime we can calculate the structure functions $F_i^{W^\pm}$ from parton dynamics by use of the factorization theorem

[2] Our normalization of F_4 differs from that in [16] by a factor of x.

[3] A typographic error in Refs. [12,16] is corrected here in the lower limit for x.

$$W^{\mu\nu} = \int \frac{d\xi}{\xi} \; f(\xi,\mu^2) \;\; \hat{\omega}^{\mu\nu}|_{p^+=\xi P_N^+}, \tag{9}$$

relating the hadronic ($W^{\mu\nu}$) and partonic ($\hat{\omega}^{\mu\nu}$) forward matrix element of the product of weak currents $\langle J^\mu J^\nu \rangle$. In Eq. (9), $f(\xi,\mu^2)$ is a parton distribution function evaluated at factorization scale μ and the parton momentum fraction ξ of the light cone momentum of the nucleon $P_N^+ \equiv (P_N^0 + P_N^z)/\sqrt{2}$. Intrinsic transverse momentum of the incoming parton is neglected throughout our discussion, i.e. $p_\perp = 0$ in Eq. (9).

For the neutrino energies of interest here, we can safely restrict the consideration to the first two quark generations. The light flavor contributions to Eq. (3) can be obtained from the $m_c \to 0$ limit of the charm production component which we will, therefore, consider first.[4] The charm production contribution to $d\sigma$ will be represented by the structure functions F_i^c. We introduce theoretical structure functions[5]

$$\mathcal{F}_i^c(x,Q^2) = (1-\delta_{i4}) \cdot s'(\overline{\eta},\mu^2) + \frac{\alpha_s(\mu^2)}{2\pi} \times \left\{ \int_{\overline{\eta}}^1 \frac{d\xi'}{\xi'} \left[H_i^q\left(\xi', \frac{Q^2}{\mu^2}, \lambda\right) s'\left(\frac{\overline{\eta}}{\xi'}, \mu^2\right) + H_i^g\left(\xi', \frac{Q^2}{\mu^2}, \lambda\right) g'\left(\frac{\overline{\eta}}{\xi'}, \mu^2\right) \right] \right\} \tag{10}$$

for scattering off the Cabibbo-Kobayashi-Maskawa- (CKM-) rotated weak eigenstate

$$s' = |V_{s,c}|^2 \;\; s + |V_{d,c}|^2 d \tag{11}$$

and its QCD evolution partner

$$g' \equiv g(|V_{s,c}|^2 + |V_{d,c}|^2) \tag{12}$$

i.e., $ds'/d\ln Q^2 = s' \otimes P_{qq} + g' \otimes P_{qg}$.

In Eq. (10) we set the renormalization scale equal to the factorization scale and

$$\overline{\eta} = \frac{\eta}{\lambda}, \quad \frac{1}{\eta} = \frac{1}{2x} + \sqrt{\frac{1}{4x^2} + \frac{M^2}{Q^2}} \tag{13}$$

is the target mass corrected slow rescaling variable. The quantity η is the Nachtmann variable [22]. The charm mass dependence is included in the dimensionless $\lambda \equiv Q^2/(Q^2 + m_c^2)$. In Eq. (10) the convolution variable ξ in Eq. (9) has been traded for $\xi' = \overline{\eta}/\xi$ which relates to the partonic c.m. system (c.m.s) energy $\hat{s} = (p+q)^2$ through $1/\xi' = \lambda(1 + \hat{s}/Q^2)$.

The theoretical structure functions in Eq. (10) are obtained from a tensor projection on the partonic $\hat{\omega}^{\mu\nu}$ and have been conveniently normalized to a simple $\mathcal{O}(\alpha_s^0)$ term. As indicated, the leading order contribution to $\mathcal{F}_4^c$ vanishes. In the presence of target mass, the physical structure functions $F_i^{W^\pm}$ in Eq. (3)—relating to a tensor projection on the hadronic $W^{\mu\nu}$—are a mixture[6] of $\mathcal{F}_i$. Explicitly in our case of charged current (CC) charm production we have

$$F_1^c = \mathcal{F}_1^c \tag{14}$$

$$F_2^c = 2\frac{x}{\lambda} \; \frac{\mathcal{F}_2^c}{\rho^2} \tag{15}$$

$$F_3^c = 2\frac{\mathcal{F}_3^c}{\rho} \tag{16}$$

$$F_4^c = \frac{1}{\lambda} \; \frac{(1-\rho)^2}{2\rho^2} \; \mathcal{F}_2^c + \mathcal{F}_4^c + \frac{1-\rho}{\rho} \; \mathcal{F}_5^c \tag{17}$$

$$F_5^c = \frac{\mathcal{F}_5^c}{\rho} - \frac{(\rho-1)}{\lambda\rho^2} \; \mathcal{F}_2^c \tag{18}$$

where

$$\rho^2 \equiv 1 + \left(\frac{2M_N x}{Q}\right)^2, \tag{19}$$

$F_i^c = F_i^c(x,Q^2)$ and $\mathcal{F}_i^c = \mathcal{F}_i^c(x,Q^2)$. These results are in agreement with Table V in Ref. [23]. They rely only on the assignment of parton light cone momentum p^+ related to the nucleon light cone momentum $p^+ = \xi P_N^+$, with $p_\perp = 0$ and $\xi = \overline{\eta}$ at leading order.

The NLO corrections $H_{i=1,\ldots,5}^{q,g}$ were first obtained in Ref. [21] and $H_{1,2,3}^{q,g}$ have been rederived in [24]. We follow these references in notation and present the full set ($i = 1,\ldots,5$) including our independently rederived $H_{4,5}^{q,g}$. The fermionic NLO coefficient functions H_i^q in Eq. (10) for charm production are calculated from the subprocess $W^+ s \to gc$ and from the one-loop correction to $W^+ s \to c$. They are given by[7]

$$H_{i=1,2,3,5}^q\left(\xi, \frac{Q^2}{\mu^2}, \lambda\right) = \left[P_{qq}^{(0)}(\xi) \ln \frac{Q^2}{\lambda \;\; \mu^2} + h_i^q(\xi,\lambda) \right] \tag{20}$$

[4]The contribution from charm production with $m_c \neq 0$ will also round up the picture of including all effects from masses of $\mathcal{O}(1\ \mathrm{GeV})$.

[5]To meet with an experimentalist's point of view, we denote functional dependence on x and Q only in the left-hand side (LHS) of Eq. (10); corresponding in theory to an exact knowledge of all mass parameters and an ideal validity of the renormalization group for observable cross sections. Residual scale (μ) dependence will be investigated below.

[6]See Ref. [23] for details on the mixing of structure functions within the tensor basis.

[7]For the ease of notation, from here on ξ will be a generic variable and no longer the light-cone momentum of Eq. (9). To strictly match Eq. (10) we should have $\xi \to \xi'$ instead.

TABLE I. Coefficients for the expansion of h_i^q in Eq. (21).

i	A_i	$B_{1,i}$	$B_{2,i}$	$B_{3,i}$
1	0	$1-4\xi+\xi^2$	$\xi-\xi^2$	$\frac{1}{2}$
2	K_A	$2-2\xi^2-\frac{2}{\xi}$	$\frac{2}{\xi}-1-\xi$	$\frac{1}{2}$
3	0	$-1-\xi^2$	$1-\xi$	$\frac{1}{2}$
5	$\frac{\lambda-1-K_A}{\lambda}$	$-1-\xi^2$	$3-2\xi-\xi^2$	$\xi-\frac{1}{2}$

where

$$P_{qq}^{(0)}(\xi)=\frac{4}{3}\left(\frac{1+\xi^2}{1-\xi}\right)_+$$

and

$$h_i^q(\xi,\lambda)=\frac{4}{3}\left\{h^q+A_i\ \ \delta(1-\xi)+B_{1,i}\ \ \frac{1}{(1-\xi)_+}+B_{2,i}\ \ \frac{1}{(1-\lambda\xi)_+}+B_{3,i}\left[\frac{1-\xi}{(1-\lambda\xi)^2}\right]_+\right\} \quad (21)$$

with

$$h^q=-\left(4+\frac{1}{2\lambda}+\frac{\pi^2}{3}+\frac{1+3\lambda}{2\lambda}\ \ K_A\right)\delta(1-\xi)-\frac{(1+\xi^2)\ln\xi}{1-\xi}+(1+\xi^2)\times\left[\frac{2\ln(1-\xi)-\ln(1-\lambda\xi)}{1-\xi}\right]_+ \quad (22)$$

and

$$K_A=\frac{1}{\lambda}\ \ (1-\lambda)\ln(1-\lambda). \quad (23)$$

The coefficients in Eq. (21) for $i=1,2,3,5$ are given in Table I. A misprint in Ref. [21] concerning A_2 was already corrected in [24]. Here, we correct a similar misprint concerning A_5.

The gluonic NLO coefficient functions H_i^g in Eq. (10) for charm production, as calculated from the subprocess $W^+g\to c\bar{s}$, are given by

$$H_{i=1,2,5}^g\left(\xi,\frac{Q^2}{\mu^2},\lambda\right)=\left[P_{qg}^{(0)}(\xi)\left(\pm L_\lambda+\ln\frac{Q^2}{\lambda\ \mu^2}\right)+h_i^g(\xi,\lambda)\right] \quad (24)$$

where

$$P_{qg}^{(0)}(\xi)=1/2\,[\xi^2+(1-\xi)^2],\quad L_\lambda=\ln\frac{1-\lambda\xi}{(1-\lambda)\xi}$$

and

TABLE II. Coefficients for the expansion of h_i^g in Eq. (25).

i	$C_{1,i}$	$C_{2,i}$	$C_{3,i}$	$C_{4,i}$
1	$4-4(1-\lambda)$	$\frac{(1-\lambda)\xi}{1-\lambda\xi}-1$	2	-4
2	$8-18(1-\lambda)+12(1-\lambda)^2$	$\frac{1-\lambda}{1-\lambda\xi}-1$	6λ	-12λ
3	$2(1-\lambda)$	0	$-2(1-\xi)$	2
5	$8-10(1-\lambda)$	$\frac{(1-\lambda)\xi}{1-\lambda\xi}-1$	4	-10

$$h_i^g(\xi,\lambda)=C_0+C_{1,i}\ \ \xi(1-\xi)+C_{2,i}+(1-\lambda)\ \ \xi\ \ L_\lambda\ \ (C_{3,i}+\lambda\ \ \xi\ \ C_{4,i}) \quad (25)$$

with

$$C_0=P_{qg}^{(0)}(\xi)\ \ [2\ln(1-\xi)-\ln(1-\lambda\xi)-\ln\xi]. \quad (26)$$

The coefficients $C_{k,i}$ are given in Table II. As in Ref. [24], they differ from those in Ref. [21] by counting—within dimensional regularization—the gluonic helicity states in D [25,26] rather than in 4 dimensions.

The structure function F_4 is insensitive to any collinear physics up to $\mathcal{O}(\alpha_s^1)$ and the corresponding coefficients $H_{i=4}^{q,g}$ are, therefore, scheme and scale-independent functions. They are given by

$$H_{i=4}^q(\xi,\lambda)=\frac{4}{3}\ \ \frac{\lambda(1-\xi)\xi[1+(1-2\lambda)\xi]}{(1-\lambda\xi)^2} \quad (27)$$

$$H_{i=4}^g(\xi,\lambda)=2\lambda\xi[1-\xi-(1-\lambda)\xi\ \ L_\lambda]. \quad (28)$$

In the limit $\lambda\to1$ ($m_c\to0$) and after an additional minimal subtraction of the collinear mass singularities in $H_{i=1,2,3,5}^g$ the $H_i^{q,g}$ reduce to the massless $\overline{\rm MS}$ coefficient functions:[8]

$$\lim_{\lambda\to1}H_i^q\left(\xi,\frac{Q^2}{\mu},\lambda\right)\Big|_{\mu^2=Q^2}=C_{F,i}^{(1)}(\xi) \quad (29)$$

$$\lim_{\lambda\to1}\left\{H_{i=1,2,4,5}^g\left(\xi,\frac{Q^2}{\mu^2},\lambda\right)\mp(1-\delta_{i4})P_{qg}^{(0)}\ln\frac{\mu^2/Q^2}{1-\lambda}\right\}\Big|_{\mu^2=Q^2}=C_{G,i}^{(1)}(\xi) \quad (30)$$

where $C_{F,i}^{(1)}$ and $C_{G,i}^{(1)}$ for $i=1,2,3$ are the massless modified minimal subtraction scheme ($\overline{\rm MS}$) coefficients in Appendix III of [26]. Extending the results in Refs. [25–27] to include $i=4,5$ and within the notation of Ref. [26] we find

[8]The choice $\mu=Q$ is made to match with the notation in [26]. Retaining a general $\mu\neq Q$ on the LHS of Eqs. (29), (30) results in the massless coefficient functions for arbitrary scale. Obviously, this amounts to adding back the $P^{(0)}\ln(Q^2/\mu^2)$ "splitting function times log" counter-terms.

$$C_{F,4}^{(1)}(\xi)=\frac{4}{3}\xi \tag{31}$$

$$C_{F,5}^{(1)}(\xi)=C_{F,2}^{(1)}(\xi) \tag{32}$$

$$C_{G,4}^{(1)}(\xi)=2\xi(1-\xi) \tag{33}$$

$$C_{G,5}^{(1)}(\xi)=C_{G,2}^{(1)}(\xi). \tag{34}$$

To calculate the light quark contributions to CC ν_τ DIS, the massless coefficient functions on the right-hand side (RHS) of Eqs. (29)–(34) are used together with the parton distribution functions (PDFs) which multiply the CKM matrix elements $|V_{i,j\neq c}|^2$ in an obvious modification ($\lambda\to 1$, $H\to C, \ldots$) of our Eq. (10). The result is added to the charm production component (10) to obtain the entire NLO structure function.

It is interesting to note that the equalities (32), (34) guarantee that the Albright-Jarlskog relation (2) is not violated in massless QCD at NLO. Equations (14)–(18) and the fact that $H_2^{q,g}\neq H_5^{q,g}$ for charm production manifest, of course, a violation of Eq. (2) in the real world of massive target hadrons and of heavy quarks interacting through QCD. This observation must actually be expected to hold at all orders as we clarify in the Appendix.

III. STRUCTURE FUNCTIONS AND CROSS SECTIONS

A. Structure functions

The Albright-Jarlskog relations [Eqs. (1) and (2)] are valid at leading order in the massless limit. Here, we show F_4 and $2xF_5-F_2$ to demonstrate violations of these relations. We use the CTEQ6 parton distributions [28] which include estimates of the uncertainties in the distributions. Thus, in Sec. III B we will be able to quantify the error in the evaluation of $\sigma_{\rm CC}(\nu_\tau N)$ that is caused by our imperfect knowledge of the PDFs. The CTEQ6 fits are provided for $\mu>\mu_0=1.3$ GeV but can be extrapolated to lower values of μ. When the factorization scale squared goes below $\mu_{\rm cut}^2=0.5$ GeV^2, though, we choose to freeze it at $\mu^2=\mu_{\rm cut}^2$. An alternate set of parton distribution functions used below is the Glück, Reya and Vogt GRV98 set [29] which evolves from $\mu_0^2=0.4$ GeV^2 with parametrizations provided above $\mu_{\rm cut}^2=0.8$ GeV^2. In principle, CTEQ6 covers the parameter space of global PDF related data within conservative errors. On the other hand, the evolution with three quark flavors (u,d,s) of GRV98 matches better with our evaluation of $\sigma_{\rm CC}(\nu_\tau N)$ at low neutrino energies where we assume light sea quarks only. In comparison, the CTEQ6 PDFs are evolved with a variable flavor number which is, strictly, not fully compatible with our approach. When we quantify the uncertainties from the PDF degrees of freedom we will, therefore, employ GRV98 for an independent comparison. Thereby, we can convince ourselves that the slight inconsistency mentioned above leads to no noticeable bias in practice. The CTEQ6 NLO $\overline{\rm MS}$ set of parton distribution functions is our default choice in the evaluations below. If not stated otherwise, the curves correspond to $\mu=Q$.

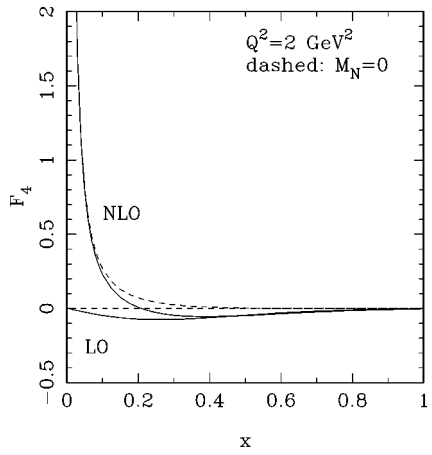

FIG. 1. The structure function F_4 as a function of x at fixed $Q^2=2$ GeV^2, at LO and NLO, using the CTEQ6 parton distribution functions. Dashed lines show the case with target mass $M_N=0$.

In Fig. 1, we show $F_4(x,Q^2=2\ \text{GeV}^2)$. The solid lines in the figure include target mass corrections of Eq. (17), while the dashed lines are with the target mass set to zero, so that $\eta\to x$ and $\rho=1$. The leading order (LO) curve with $M_N=0$ shows $F_4=0$, even with charm mass corrections included. A leading order violation would occur if the initial quark masses were set to nonzero values. Including the target mass corrections shows the effect of the mixing of $\mathcal{F}_4$ with $\mathcal{F}_2$ and $\mathcal{F}_5$ in Eq. (17). The NLO corrections have an effect primarily at small x.

Figure 2 shows the violation of the second Albright-Jarskog relation, at fixed $Q^2=2$ GeV^2. Even at leading order, $2xF_5-F_2\neq 0$. This is due to charm quark mass corrections in $W^+s'\to c$. The magnitude at small x reflects the impact of the s' sea distribution. Target mass effects incorporated by Eq. (18) are not significant. Including the NLO corrections makes small changes to the curve at small x. Both of the figures show that in evaluations of the total

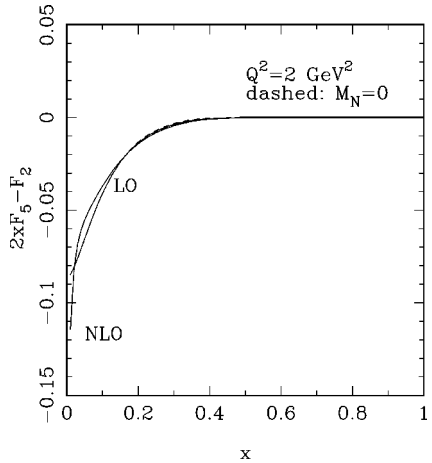

FIG. 2. The structure function difference $2xF_5-F_2$ as a function of x at fixed $Q^2=2$ GeV^2, at LO and NLO, using the CTEQ6 parton distribution functions. Dashed lines show the case with target mass $M_N=0$.

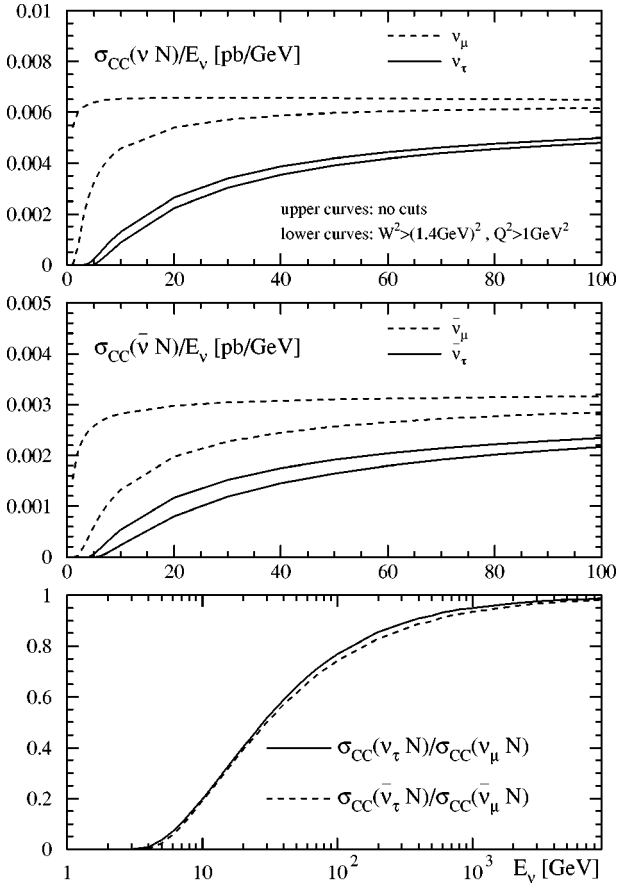

FIG. 3. Cross sections for inclusive neutrino [$\sigma_{CC}(\nu N)$, upper panel] and anti-neutrino [$\sigma_{CC}(\bar{\nu}N)$, middle panel] production of charged leptons on an isoscalar target, evaluated at NLO and plotted versus the energy of incident μ- and τ-flavored (anti-)neutrinos. We show the outcome of a naive integration over the full kinematic range of W^2 and Q^2 along with the effect of imposing DIS cuts on these variables. The ratios $\sigma_{CC}(\nu_\tau N)/\sigma_{CC}(\nu_\mu N)$ and $\sigma_{CC}(\bar{\nu}_\tau N)/\sigma_{CC}(\bar{\nu}_\mu N)$ which we show in the lower panel are insensitive to these cuts (and we show the uncut results).

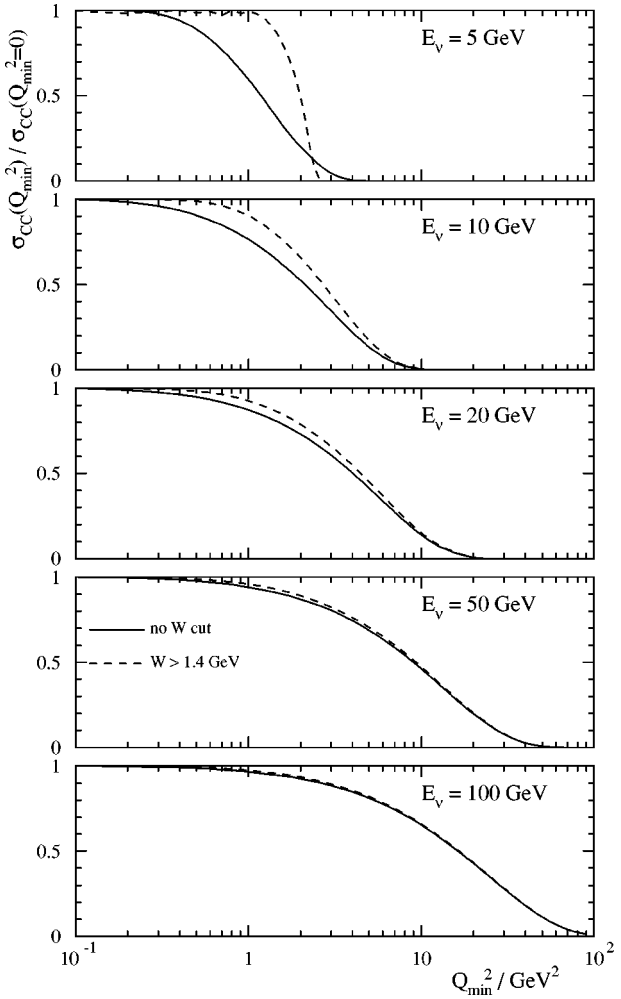

FIG. 4. Ratio $\sigma_{CC}(Q^2_{min})/\sigma_{CC}(Q^2_{min}=0)$ versus Q^2_{min} for $\nu_\tau N$ CC interactions with $E_\nu=5$, 10, 20, 50 and 100 GeV. The solid lines are with $W_{min}=0$, the dashed lines with $W_{min}=1.4$ GeV.

charged current cross section, the naive Albright-Jarlskog relations are good approximations to the NLO results. This is true at low energies, where $\sigma_{CC}(\nu_\tau N)$ does not probe small-x and at high energies where $F_{4,5}$ are suppressed, anyway.

B. Cross sections

The cross sections for neutrino and antineutrino charged current interactions with isoscalar nucleons are shown in the first two panels of Fig. 3. We use our default set of CTEQ6 parton distribution functions with the factorization scale equal to the renormalization scale μ^2 and $\mu^2=Q^2$. Below $\mu^2=\mu^2_{cut}$, we set $\mu^2=\mu^2_{cut}$ in the parton distribution functions and in α_s, but we keep the explicit Q^2 dependence in the differential cross section of Eq. (3) as well as in the counter-logs $\sim \ln Q^2/\mu^2_{cut}$ of the NLO coefficient functions. For $Q^2<\mu^2_{cut}$, a noticeable impact of these logs is indicative of long-distance strong interaction. The evaluation can, therefore, not be trusted perturbatively, whenever it becomes sensitive to the technical choice $\mu>\mu_{cut}$. Most of our results below are, however, completely insensitive to it. In Fig. 3 muon (anti-)neutrino cross sections appear with dashed lines, while the solid lines show the tau (anti-)neutrino cross sections. The upper curves show no cuts while the lower curves have $W^2=Q^2(x^{-1}+1)+M_N^2>(1.4\ \text{GeV})^2$ and $Q^2>1\ \text{GeV}^2$. As we show in Fig. 4, for $W_{min}=1.4$ GeV, the tau neutrino CC cross section is fairly insensitive to the Q^2 cut of 1 GeV^2. At, for example, $E_\nu=20$ GeV, $\sigma_{CC}(Q^2_{min}=1\ \text{GeV}^2)/\sigma_{CC}(Q^2_{min}=0)=0.93$ for $\nu_\tau N$ CC interactions. The Q^2 cut has a larger impact on $\sigma_{CC}(\nu_\mu N)$, where $\sigma_{CC}(Q^2_{min}=1\ \text{GeV}^2)/\sigma_{CC}(Q^2_{min}=0)=0.85$ for $E_\nu=20$ GeV, due to the fact that for nearly massless leptons, $Q^2>Q^2_{min}$ cuts out a larger fraction of the available phase space.

The small changes in the CC cross sections with $Q^2_{min}=1\ \text{GeV}^2$ lead one to expect that nonperturbative effects at low Q^2 are unlikely to be large when one also applies the W_{min} cut of 1.4 GeV. At low energies, without the W_{min} cut, a substantial contribution to the cross sections comes from $Q^2<1\ \text{GeV}^2$, however, and this is precisely where the DIS cross section is only a rough approximation to the true cross sections with quasi-elastic and resonant as well as nonresonant contributions.

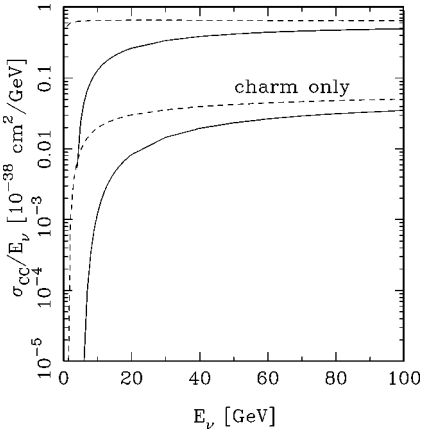

FIG. 5. The charged current cross section and the separate contribution from $\nu N \to cX$ for incident ν_μ (dashed line) and ν_τ (solid line). At $E_\nu = 100$ GeV, the charm production contribution is about 7% of the total.

The bottom panel of Fig. 3 shows the ratio of the $\nu_\tau N$ to $\nu_\mu N$ CC cross sections (solid lines) and the same ratio for antineutrinos. Shown are the uncut results, but the results with the $W_{\min}$ and Q^2 cuts agree to within 3% for $E_\nu > 20$ GeV. Of note is the fact that even at $E_\nu = 10^3$ GeV, the $\nu_\tau N$ to $\nu_\mu N$ CC cross section ratio is still 5% below unity. At 100 GeV, the ratio is 0.76. There are two reasons for the deficit in the ν_τ CC cross section: the reduced phase space and the contribution of F_5. The reduced phase space is reflected in the integration limits for x and y [Eqs. (6) and (7)] [30]. This is responsible for about half of the suppression of the ν_τ CC cross section relative to $\sigma_{\rm CC}(\nu_\mu N)$. In Eq. (3), the F_5 term appears with a minus sign, and no factor of x. Since $F_5 \sim F_1 \sim q(x,Q^2)$, there is a small-$x$ enhancement of its contribution to the cross section at high energies. The F_5 term accounts for the rest of the suppression of the ν_τ cross section at high energies. The tau mass corrections to the prefactors of F_1, F_2 and F_3 become negligible at high energies because the low-x rise of $q(x)$ is tempered by factors of x or y for these structure function.

Since mass effects for tau neutrino interactions persist to 1 TeV, it is interesting to compare to the case of muon neutrino CC interactions at low energies where the muon mass is important. Since the factor of lepton mass comes into the equations via m_τ^2/E_ν, the energy for muon neutrino interactions equivalent to 1 TeV for ν_τ is $E_\nu = 3.5$ GeV. At this energy, $\sigma_{\rm CC}(\nu_\mu N)$ including $m_\mu = 0.106$ GeV (without cuts) is 2% lower than the cross section with $m_\mu = 0$. This smaller suppression is due to the fact that at low energies, one does not get significant small-x contributions to F_5. Furthermore, for $\nu_\mu N$ scattering, this energy is in the range where the DIS approximation to the total cross section is not reliable.

Charm production in neutrino interactions is a small contribution. In Fig. 5, we show the total charged current cross section and the separate cross section for $\nu N \to cX$ as a function of incident neutrino energy. The dashed curves are for incident ν_μ, the solid curves for incident ν_τ. At $E_\nu = 100$ GeV, charm production contributes about 7% of the cross section for both ν_μ and ν_τ.

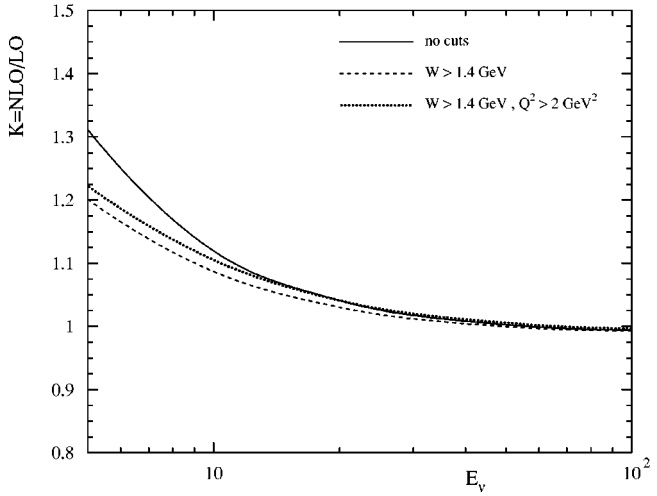

FIG. 6. The K factor $K = \text{NLO/LO}$ for tau neutrinos with no cuts (solid), $W_{\min} = 1.4$ GeV (long dash) and $W_{\min} = 1.4$ GeV with $Q^2 > 2$ GeV^2 (short dash).

The K factor, a comparison of the NLO to LO[9] charged current cross sections for incident tau neutrinos is shown in Fig. 6. As to be expected, NLO corrections are most significant near threshold where virtualities Q^2 are lower and α_s is larger than at higher energies. At $E_\nu = 10$ GeV, $K = \text{NLO/LO} = 1.12$, reducing to $K = 1$ at $E \simeq 50$ GeV for the evaluation with no cuts. The three curves show that with $W_{\min} > 1.4$ GeV and $Q^2 > 2$ GeV^2, K factor is the same as for the uncut cross section except for $E_\nu < 10$ GeV where the cuts improve the perturbative convergence. The K factor with only the $W_{\min}$ cut is even slightly lower, confirming the expectation based on Fig. 4 that perturbation theory is well behaved and its convergence does not have to be improved by any further $Q_{\min}$ cut on top of $W_{\min}$. Overall, the K factor is reasonably close to one to indicate trustworthy perturbative NLO predictions, even more so when the $W_{\min}$ cut is imposed.

C. Uncertainties

In this section we investigate a few factors that cause theoretical errors in the evaluation of $\sigma_{\rm CC}$. A full assessment of uncertainties will have to be based on the combination of the quasi-elastic and resonant channels with our DIS results. At higher energies, though, where DIS becomes dominant, we already can provide a good guide towards error estimates.

An uncertainty in our evaluation of the cross section is due to the factorization scale dependence of the cross section at fixed order in perturbation theory. To evaluate the uncertainty due to the scale dependence, we have varied the factorization and renormalization scale ($\mu = \mu_F = \mu_R$) over a very wide range of $\mu^2 = 0.1 - 10\ Q^2$ for energies between 5 GeV and 100 GeV. A selection of energies is shown in Fig. 7. We show the ratio of $\sigma_{\rm CC}(\nu_\tau N)$ as a function of μ^2/Q^2 to the cross section at $\mu^2 = Q^2$. The flat μ dependence is a

[9]The LO result is obtained by neglecting all $\mathcal{O}(\alpha_s^1)$ terms in Sec. II and employing the CTEQ6L PDFs.

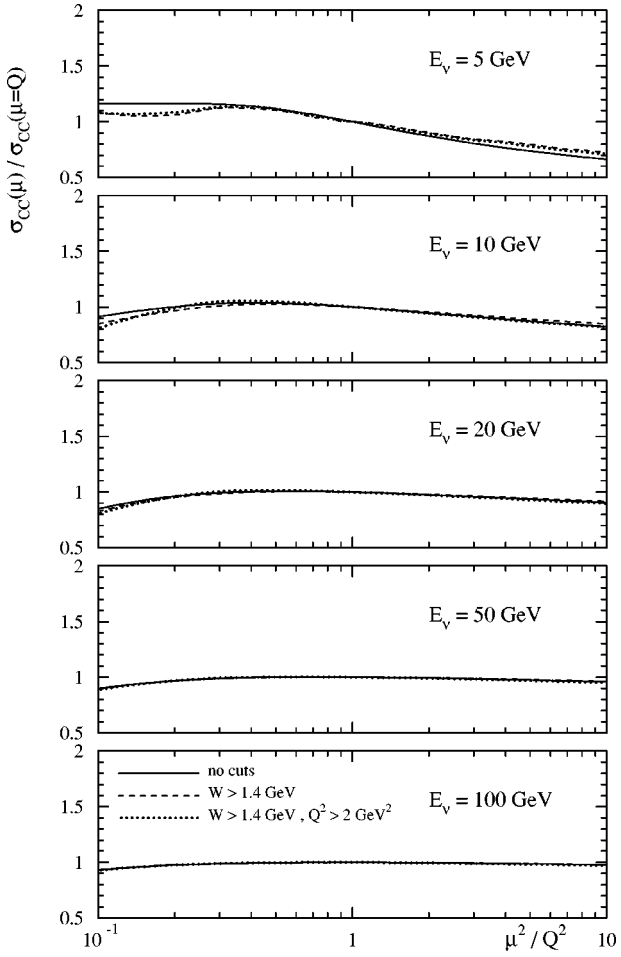

FIG. 7. The ratio of $\sigma_{CC}(\mu)/\sigma_{CC}(\mu=Q)$ in NLO for ν_τN interactions, as a function of μ^2/Q^2 for several values of E_ν.

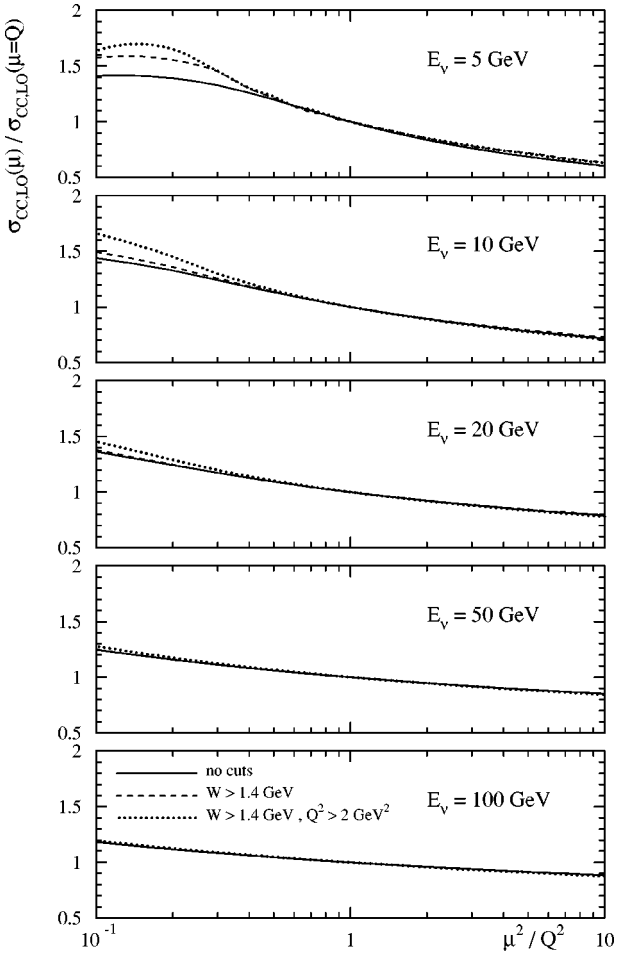

FIG. 8. The ratio of $\sigma_{CC}(\mu)/\sigma_{CC}(\mu=Q)$ in LO for ν_τN interactions, as a function of μ^2/Q^2 for several values of E_ν.

reassuring feature of the NLO calculation as opposed to the monotonic decrease with μ observed in LO, see Fig. 8. While we discuss here the full range of μ^2 as plotted in Fig. 7, the perturbative stability observed in Fig. 6 suggests that one would very likely overestimate the uncertainty from higher orders by such a wide scale variation. This seems even more so if we look at the scale dependent K factor in Fig. 9 which prefers scales close to the canonical DIS choice $\mu=Q$ where $K\simeq 1$. Still, scale choices are arbitrary to a large extent and we prefer to discuss the full picture instead of narrowing it down to some window for μ around $\mu=Q$. At $E_\nu=5$ GeV, the variation is the largest for the cross section evaluated with no cuts, ranging between 1.16 and 0.66. As explained in Sec. III A, for $\mu^2<\mu_{\rm cut}^2$, we always set $\mu=\mu_{\rm cut}$.[10] For small μ/Q, the ratio without cuts in $\{W,Q\}$ is nearly constant as a function of μ^2/Q^2, showing the degree to which the uncut cross section comes from small μ values where $\mu_{\rm cut}$ takes over and where the perturbative treatment is unreliable. With $\{W,Q\}$ cuts applied, the variation over the range of scales is slightly less. The scale uncertainty at low energies underlies a larger uncertainty associated with the DIS approximation near threshold where the quasi-elastic and resonant contributions are significant.

At higher energies, the variation in the ratio is between $\sim 0.85-1$. For $E_\nu=20$ GeV, the ratio in Fig. 7 is between 0.95 and 1 for $\mu^2/Q^2\sim 0.2-4$.

The uncertainty in the cross section due to uncertainties in the parametrization of the parton distribution functions (PDF) is harder to quantify than the scale dependence. One approach is to use different parton distribution functions than the default CTEQ6 set. As a comparison, the Glück-Reya-Vogt 1998 (GRV98) PDF set, at $E_\nu=20$ GeV with $\mu=Q$, yields a cross section only about one percent smaller than the CTEQ6 set. At $E_\nu=5$ and 10 GeV, the GRV98 cross sections are 10% and 4% lower than the CTEQ6 cross sections when no cuts are applied. The larger deviation at lower energies is due to the different high-x distributions in the two PDF sets. Including $W>1.4$ GeV results in a deviation of 3.6% at $E_\nu=5$ GeV, even less for higher energies. Table III represents results for a few selected energies with a cut in W applied. As commented above in Sec. III A, the PDFs also differ in their treatment of the number of active flavors and in the value of the strong coupling constant.

[10] I.e., strictly the plot should be labeled $\sigma_{CC}(\max\{\mu,\mu_{\rm cut}\})/\sigma_{CC}(\max\{Q,\mu_{\rm cut}\})$.

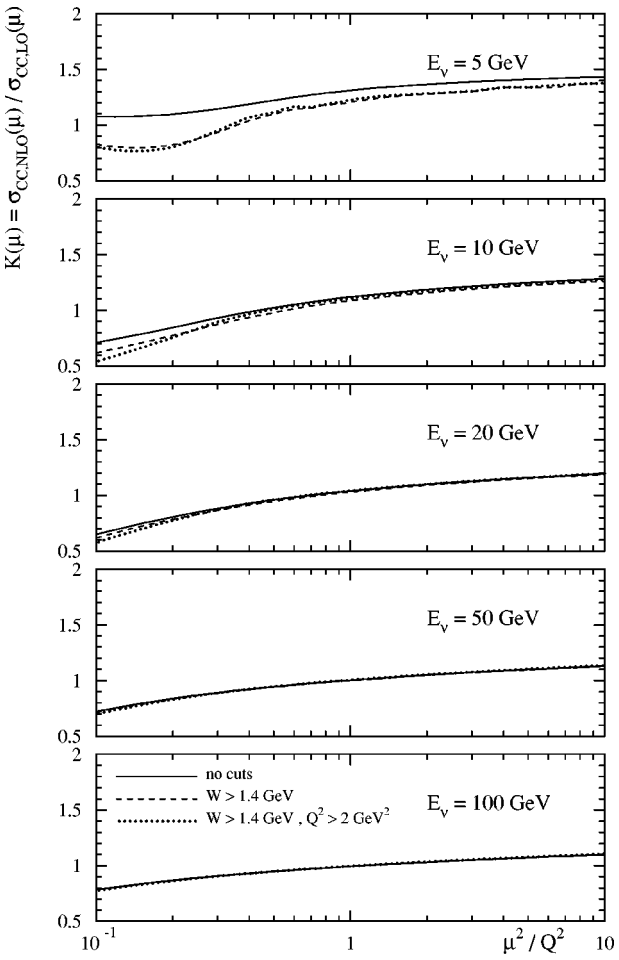

FIG. 9. The K factor $K=\mathrm{NLO/LO}$ versus factorization scale μ for tau neutrinos with no cuts (solid), $W_{\min}=1.4$ GeV (long dash) and $W_{\min}=1.4$ GeV with $Q^2>2$ GeV^2 (short dash).

The CTEQ Collaboration has also provided distributions in addition to their best fit set [28]. The 20 dimensional parameter space to which the PDFs are sensitive yields 40 PDF sets with plus/minus variations on the eigenvector directions in that space. The resulting error estimate on $\sigma_{\mathrm{CC}}(\nu_\tau N)$ from evaluating the 40 sets is 3% at $E_\nu=20$ GeV, see Table III for other values of E_ν. Overall, the GRV98 results lie within the uncertainty estimate suggested by the CTEQ6 eigenvector PDFs. We can, therefore, be confident of the absence of a systematic effect from the number of flavors and that the statistical uncertainties as encoded in the CTEQ6 sets provide a realistic PDF error estimate for $\sigma_{\mathrm{CC}}(\nu_\tau N)$.

TABLE III. Propagation of PDF uncertainties into the evaluation of $\sigma_{\mathrm{CC}}(\nu_\tau N)$ with a cut $W>1.4$ GeV. The second column $\Delta\sigma_{\mathrm{CC}}$ was calculated using the CTEQ6 eigenvector PDFs along the master formula (3) in [28]. The third column compares GRV98 [29] with the central CTEQ6M set.

E_ν [GeV]	$\Delta\ \sigma_{\mathrm{CC}}$	$\sigma_{\mathrm{CC}}(\mathrm{GRV98})-\sigma_{\mathrm{CC}}(\mathrm{CTEQ6})$
5	5.6%	−3.6%
10	3.3%	−2.5%
20	2.8%	−1.0%
50	2.4%	±0.0%
100	2.2%	+0.5%

We have incorporated kinematic corrections due to including the target hadron mass M_N by employing the parton light cone fraction ξ, which equals the Nachtmann variable η [22] at leading order in the massless quark limit. One finds that η is much different than Bjorken-x at large x. For example, for $Q^2=2$ (10) GeV^2, $\eta=0.45$ (0.49) at $x=0.5$ and $\eta=0.75$ (0.92) at $x=1$. The use of η rather than x in the structure functions has the largest impact at high x and low Q^2.

Target mass corrections are also included via Eqs. (14)–(18), in which the $\mathcal{F}_i$ are mixed with target mass dependent prefactors for a given F_i. These formulas are based on the assignment of $p_+=\xi P_+$ to the light-cone momentum of the massless incident parton ($p^2=0$) given $P^2=M_N^2$. The parton and nucleon are assumed to have collinear momenta, $p_\perp=0$. The formalism is discussed in detail in Ref. [23], however, other choices for the model of including target mass effects are possible, for example, including parton transverse momentum [31] $p_\perp\neq 0$. The model of Ref. [31] reproduces the kinematic corrections for the leading twist operator product expansion result [32]. As a consequence, our results here serve only as a guide to the magnitude of target mass corrections to the charged current cross sections. For the transverse structure function F_T of Ref. [31], which equals $\mathcal{F}_2$ in the collinear parton approximation, the difference between the $p_\perp\neq 0$ approximation giving F_T and our order $p_\perp^0$ approximation is less than 10% over all x and Q^2 as low as 1 GeV^2, rapidly falling below 5% at $Q^2=2$ GeV^2. Low energy $\mathcal{O}(p_\perp^2)$ effects and the target mass treatment in general border onto dynamical higher twists at large-x [33–35]. Those concepts will be investigated in more detail when future work will combine the DIS cross sections with the non-DIS channels.

The effects of the target mass corrections as implemented here on F_4 and $2xF_5-F_2$, as shown in Figs. 1 and 2, are small. In terms of the total cross section, the lowest energies are most affected. In the absence of kinematic cuts, $\sigma_{\mathrm{CC}}(\nu_\tau N)(E_\nu=10\ \mathrm{GeV})$ for $M_N=0$ is 8% larger than the cross section including the target mass via η and Eqs. (14)–(18). For $E>20$ GeV, the deviation is less than 5%, down to the 2% level at 50 GeV incident neutrino energy. When one includes $W>W_{\min}=1.4$ GeV, the effect of target mass corrections on the $\nu_\tau N$ CC cross section is less than 2% for $E_\nu>8$ GeV. The reduced effect is due to the fact that the $W_{\min}$ value reduces the region of integration for large x since $2M_NE_\nu y(1-x)\geqslant W_{\min}^2-M_N^2$.

IV. CONCLUSIONS

The NLO corrections for the $\nu_\tau N$ charged current cross section have a relatively large impact at low neutrino energies near threshold and less of an impact at high energies. We have already shown the K factor in Fig. 6. In Fig. 10, we show $\sigma_{\mathrm{CC}}(\nu_\tau N)/E_\nu$ versus neutrino energy at NLO including target mass corrections as implemented via Eqs. (14)–

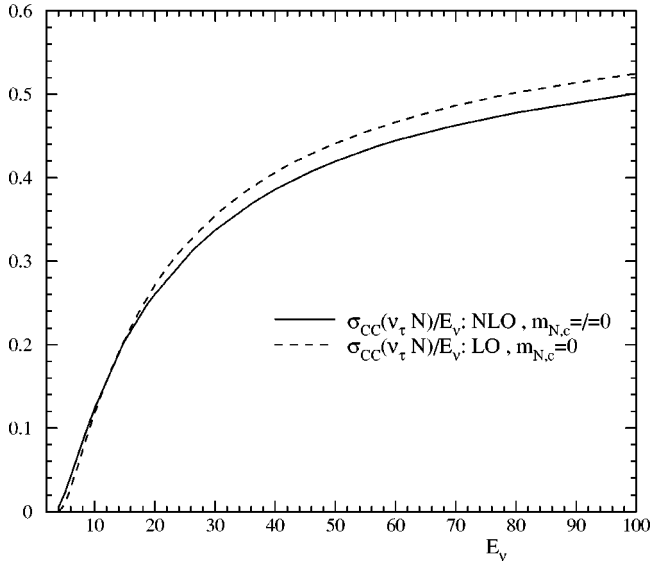

FIG. 10. Our calculation of $\sigma_{\rm CC}(\nu_\tau N)/E_\nu$ (10^{-38} cm^2/GeV) versus neutrino energy (GeV) compared to its naive evaluation neglecting masses and NLO corrections.

(18) and charm mass correction. This is compared to the naive evaluation, neglecting masses and NLO corrections, where the Albright-Jarlskog relations are correct. At high energies, the target mass corrections are negligible. The main effect is due to the charm mass threshold. At lower energies, the larger QCD K factor is compensated by the reduction in the cross section due to target mass and charm mass effects.

In the theoretical evaluation of the $\nu_\tau N$ charged current cross section, the scale dependence in the PDFs and α_s is a large uncertainty at low energies. The parametrization of the PDFs does not seem to be a large uncertainty in the evaluation of the total cross section, especially when one applies DIS cuts on W^2 and Q^2.

Target mass corrections and the importance of $Q^2 < 1$ GeV^2 are small at high energies, but they are significant in the 10–20 GeV energy range and lower, especially for the cross section without kinematic cuts. Our implementation of target mass corrections neglects parton transverse momentum ($p_\perp^2$). This approach makes the inclusion of NLO QCD corrections straightforward, however, it neglects corrections of order M_N^2/Q^2 induced by nonzero $p_\perp^2$ [31]. As a consequence, one should view our target mass corrections as approximate.

In any case, the DIS cross section in the energy region below $E_\nu \sim 10-20$ GeV is difficult to interpret. At best, the uncut cross section is a crude approximation to the total cross section including resonant hadron production, e.g., Δ production. The cross section with cuts is likely a better representation of the nonresonant neutrino-nucleon interactions, however, the issue of avoiding double counting in combining resonant and nonresonant interactions is not solved theoretically. Phenomenological approaches are being explored [13] for applications to $\nu_\mu N$ interactions in the few GeV region that may also be applied to $\nu_\tau N$ interactions at higher energies. The universality of M_N^2/Q^2 corrections, carried over from copious electromagnetic interaction data to the context of weak interactions, is not completely clear.

The νN cross section is an important ingredient in current and future atmospheric and neutrino factory experiments. Our evaluation of the NLO corrections for ν_τN CC interactions including charm mass corrections and an estimate of target mass effects is part of a larger theoretical program [12–17,21] to understand the inelastic νN cross section over the full energy range relevant to current and future experiments.

ACKNOWLEDGMENTS

We thank K. Ellis, M. Goodman, R. Jakob, F. Olness, W.K. Tung and U.K. Yang for discussions. This research was supported in part by the National Science Foundation under Grants PHY-0070443 and PHY-9802403 and DOE Contract No. FG02-91ER40664.

APPENDIX: THE ALBRIGHT-JARLSKOG RELATIONS

In this appendix we pinpoint the approximations for which the Albright-Jarlskog relations (AJRs) (1) and (2) hold beyond the naive parton model (where they are exact). Below, we will rewrite the AJRs in terms of helicity amplitudes. First, however, we can immediately tell from Eqs. (14)–(18) that the mixing of $\{\mathcal{F}_2^c, \mathcal{F}_4^c, \mathcal{F}_5^c\}$ for $M_N \neq 0$ will violate both Eqs. (1) and (2). We will, therefore, restrict the following discussion to $M_N = 0$. The charm mass will be retained to trace its (somewhat less obvious) impact on the AJRs. In terms of helicity projections

$$W_0 = \varepsilon_0^\mu \varepsilon_0^\nu W_{\mu\nu} \tag{A1}$$

$$W_s = (\varepsilon_0^\mu \varepsilon_q^\nu + \varepsilon_q^\mu \varepsilon_0^\nu) W_{\mu\nu} \tag{A2}$$

$$W_q = \varepsilon_q^\mu \varepsilon_q^\nu W_{\mu\nu} \tag{A3}$$

$$W_\pm = \varepsilon_\pm^\mu \varepsilon_\pm^{\nu\,*} W_{\mu\nu} \tag{A4}$$

with polarization vectors in terms of virtual W momentum q and longitudinal reference vector k

$$\varepsilon_\pm^\mu = \frac{1}{\sqrt{2}}\ (0, \mp 1, -i, 0)\ \text{(transverse)} \tag{A5}$$

$$\varepsilon_q^\mu = \frac{q^\mu}{\sqrt{-q^2}}\ \text{(scalar)} \tag{A6}$$

$$\varepsilon_0^\mu = \frac{(-q^2)k^\mu + (k\cdot q)q^\mu}{\sqrt{(-q^2)[(k\cdot q)^2]}}\ \text{(longitudinal)}, \tag{A7}$$

the tensor basis $\mathcal{F}^c_{i=1,\ldots,5}$ can be written as

$$\mathcal{F}_1^c = \frac{1}{2}(W_+ + W_-) \tag{A8}$$

$$\mathcal{F}_2^c = \frac{\lambda}{2}(W_+ + W_- + 2W_0) \tag{A9}$$

$$\mathcal{F}_3^c = \mp\frac{1}{2}(W_+ - W_-) \tag{A10}$$

$$\mathcal{F}_4^c = \frac{1}{2}(W_0 + W_q - W_s) \tag{A11}$$

$$\mathcal{F}_5^c = \frac{1}{2}(W_+ + W_- + 2W_0 - W_s). \tag{A12}$$

We then see that

$$F_2^c - 2xF_5^c = 2\frac{x}{\lambda}\mathcal{F}_2^c - 2x\mathcal{F}_5^c = xW_s \tag{A13}$$

singles out the interference term W_s between scalar and longitudinal polarization. The latter involves a contraction with $\varepsilon_q^\mu \propto q^\mu$. Now, as long as we make the single W boson exchange approximation, the DIS process is equivalent to an effectively abelian (electroweak) interaction *if* all quarks are massless (or of the same mass). Then, $F_2 - 2xF_5 = 0$ is guaranteed by naive gauge invariance under $\varepsilon_q^\mu \to \varepsilon_q^\mu - q^\mu/\sqrt{-q^2} = 0^\mu$. This is a stronger statement than helicity conservation for massless spin-1/2 quarks because gauge invariance holds to any order in α_s while helicity conservation breaks down when noncollinear NLO radiation generates angular momentum. A transition $W^+ s \to c$ with $0 = m_s \neq m_c$, however, is necessarily nondiagonal in flavor space and the interaction cannot be abelianized. Thus, naive gauge invariance does not hold and the second AJR (2) is not protected from charm mass corrections. It will, however, hold at any order in α_s for massless quarks.

Worth mentioning also is that $F_4^c = 0$ at $\mathcal{O}(\alpha_s^0)$ even for the charm production process, indicating that $W_0 + W_q - W_s = 0$ at LO. This should be compared to the longitudinal structure function $F_2 - 2xF_1 \propto W_0$ which does not vanish by helicity conservation in LO when a massive charm quark is produced in the final state. Now, F_4 is obtained from

$$W_0 + W_q - W_s = \frac{k^\mu k^\nu}{Q^2} W_{\mu\nu}. \tag{A14}$$

At the parton level, k is the *incoming* parton momentum p. F_4 does, therefore, not receive corrections from the final state charm mass in LO as long as initial state down and strange masses are zero ($p^2 = 0$).

[1] Super-Kamiokande Collaboration, Y. Fukuda *et al.*, Phys. Lett. B **436**, 33 (1998); Super-Kamiokande Collaboration, Y. Fukuda *et al.*, Phys. Rev. Lett. **81**, 1562 (1998).

[2] IceCube Collaboration, J. Ahrens *et al.*, "IceCube Preliminary Design Document," at http://icecube.wisc.edu/; AMANDA Collaboration, A. Biron, Part. Nucl. Lett. **106**, 7 (2001); ANTARES Collaboration, T. Montaruli, Nucl. Phys. B (Proc. Suppl.) **110**, 513 (2002); BAIKAL Collaboration, B.K. Lubsandorzhev, Part. Nucl. Lett. **106**, 21 (2001); NESTOR Collaboration, P.K. Grieder, Nuovo Cimento Soc. Ital. Fis., C **24C**, 771 (2001).

[3] A. Rubbia, Nucl. Phys. B (Proc. Suppl.) **91**, 223 (2000); ICARUS and NOE Collaboration, F. Arneodo *et al.*, "ICANOE: Imaging and calorimetric neutrino oscillation experiment," LNGS-P21/99, INFN/AE-99-17, Report No. CERN/SPSC 99-25, SPSC/P314; OPERA COLLABORATION, M. Guler *et al.*, Report No. CERN/SPSC 2000-028, SPSC/P318, LNGS-P25/2000; MONOLITH Collaboration, F. Terranova, Int. J. Mod. Phys. A **16S1B**, 736 (2001); V. Paolone, Nucl. Phys. B (Proc. Suppl.) **100**, 197 (2001).

[4] C. Albright *et al.*, hep-ex/0008064.

[5] A. Devoto, D.W. Duke, J.D. Kimel, and G.A. Sowell, Phys. Rev. D **30**, 541 (1984); D.W. Duke, J.D. Kimel, and G.A. Sowell, *ibid.* **25**, 71 (1982).

[6] E.B. Zijlstra and W.L. van Neerven, Phys. Lett. B **297**, 377 (1992); Nucl. Phys. **B383**, 525 (1992); Phys. Lett. B **273**, 476 (1991); **272**, 127 (1991).

[7] D.I. Kazakov, A.V. Kotikov, G. Parente, O.A. Sampayo, and J. Sanchez Guillen, Phys. Rev. Lett. **65**, 1535 (1990).

[8] S.A. Larin and J.A. Vermaseren, Z. Phys. C **57**, 93 (1993).

[9] S.A. Larin, P. Nogueira, T. van Ritbergen, and J.A. Vermaseren, Nucl. Phys. **B492**, 338 (1997); S.A. Larin, T. van Ritbergen, and J.A. Vermaseren, *ibid.* **B427**, 41 (1994).

[10] A. Retey and J.A. Vermaseren, Nucl. Phys. **B604**, 281 (2001).

[11] W.L. van Neerven and A. Vogt, J. Phys. G **28**, 727 (2002); Phys. Lett. B **490**, 111 (2000); Nucl. Phys. **B588**, 345 (2000); **B568**, 263 (2000).

[12] E.A. Paschos and J.Y. Yu, Phys. Rev. D **65**, 033002 (2002).

[13] A. Bodek and U.K. Yang, Nucl. Phys. B (Proc. Suppl.) **112**, 70 (2002).

[14] H.M. Gallagher and M.C. Goodman, NuMI note NuMI-112, 1995, http://www.hep.anl.gov/ndk/hypertext/numi_notes.html.

[15] S. Dutta, R. Gandhi, and B. Mukhopadhyaya, Eur. Phys. J. C **18**, 405 (2000).

[16] C.H. Albright and C. Jarlskog, Nucl. Phys. **B84**, 467 (1975).

[17] P. Lipari, M. Lusignoli, and F. Sartogo, Phys. Rev. Lett. **74**, 4384 (1995).

[18] C.H. Llewellyn Smith, Phys. Rep. **3**, 261 (1972); L.A. Ahrens *et al.*, Phys. Rev. D **35**, 785 (1987).

[19] D. Rein and L.M. Sehgal, Ann. Phys. (N.Y.) **133**, 79 (1981); G.L. Fogli and C. Nardulli, Nucl. Phys. **B160**, 116 (1979); **B165**, 162 (1980); E.A. Paschos, L. Pasquali, and J.Y. Yu, *ibid.* **B588**, 263 (2000).

[20] For examples of Monte Carlo computer simulations incorporating the various contributions to the neutrino nucleon cross section, see e.g., D. Casper, Nucl. Phys. B (Proc. Suppl.) **112**, 161 (2002); and A. Rubbia *et al.*, "NUX-neutrino generator," http://neutrino.kek.jp/nuint01/.

[21] T. Gottschalk, Phys. Rev. D **23**, 56 (1981).

[22] O. Nachtmann, Nucl. Phys. **B63**, 237 (1973).

[23] M.A.G. Aivazis, F.I. Olness, and W.-K. Tung, Phys. Rev. D **50**, 3085 (1994).

[24] M. Glück, S. Kretzer, and E. Reya, Phys. Lett. B **380**, 171 (1996); **405**, 391E (1996).

[25] W.A. Bardeen, A.J. Buras, D.W. Duke, and T. Muta, Phys. Rev. D **18**, 3998 (1978).
[26] W. Furmanski and R. Petronzio, Z. Phys. C **11**, 293 (1982).
[27] G. Altarelli, R.K. Ellis, and G. Martinelli, Nucl. Phys. **B157**, 461 (1979).
[28] J. Pumplin, D.R. Stump, J. Huston, H.L. Lai, P. Nadolsky, and W.K. Tung, J. High Energy Phys. **07**, 012 (2002).
[29] M. Glück, E. Reya, and A. Vogt, Eur. Phys. J. C **5**, 461 (1998).
[30] N.I. Starkov, J. Phys. G **27**, L81 (2001).
[31] R.K. Ellis, W. Furmanski, and R. Petronzio, Nucl. Phys. **B212**, 29 (1983); **B207**, 1 (1982).
[32] H. Georgi and H.D. Politzer, Phys. Rev. D **14**, 1829 (1976).
[33] A. De Rùjula, H. Georgi, and H.D. Politzer, Phys. Rev. D **15**, 2495 (1977).
[34] P.W. Johnson and W.K. Tung, in *Neutrino 79: Proceedings*, edited by A. Haatuft and C. Jarlskog (Bergen University, Bergen, Norway, 1979), Vol. 2, pp. 612–621; K. Bitar, P.W. Johnson, and W.K. Tung, Phys. Lett. **83B**, 114 (1979).
[35] A. Piccione and G. Ridolfi, Nucl. Phys. **B513**, 301 (1998).